



Directional soft jumper by harnessing asymmetric snapping of a semi-open shell

Min Li ^{a,b,*}, Huikai Zhang ^b, Wei Fang ^b, Jian Wu ^b, Xi-Qiao Feng ^{b,**}

^a College of Mechanics and Engineering Science, Hohai University, Nanjing 210024, China

^b Institute of Biomechanics and Medical Engineering, Department of Engineering Mechanics, Tsinghua University, Beijing 100084, China

ARTICLE INFO

Keywords:

Soft robot
Soft actuator
Directional jump
Snapping-through buckling
Instability

ABSTRACT

Precise control of the jumping direction and trajectory of soft robotics poses a challenge due to their large deformation and low stiffness. In this paper, we propose a pneumatic soft actuator consisting of an inward semi-spherical shell with a pre-existing T-shaped incision, which exhibits asymmetric snapping-through buckling under an increasing internal pressure. During the dynamic snapping, the shell deforms rapidly, resulting in an asymmetric, inclined impact with the ground. The impact force drives the soft actuator to jump in a controllable direction, and the adopted semi-open pneumatic system greatly improves the efficient utilization of air ejection energy. This design not only enhances the jumping performance, but also allows the control of the trajectory through adjusting the air pressure. Our experiments demonstrate that the actuator can achieve various jumping functions, for examples, to jump over obstacles of varying heights and depths, to execute rapid and continuous locomotion, and even to escape from a deep bottle. This work offers a paradigmatic idea for designing highly maneuverable and controllable soft robots.

1. Introduction

Soft robots have gained many important applications as, for example, invasive surgery tools [1,2], wearable hand-assist robots [3,4], grippers [5–8], and field explorers [9] due to their advantages of cost-effectiveness, safety in interacting with humans, and adaptability to complex working conditions. To cope with a wide range of environments, soft robots have been developed to perform various locomotion modes, such as crawling [10–12], jumping [13–18], running [19,20], rolling [21,22], and swimming [23–26].

Among the various modes of locomotion, jumping is particularly advantageous for navigating obstacles and maneuvering through unstructured environments. A few strategies have been proposed to drive the jumping of soft robots, for example, explosion [27], combustion [28,29], and elastic energy release [13,16,30]. The combustion of flammable gas can create a rapid and large internal pressure increase in the soft actuator. The strategy of elastic energy release creates large deformation in two steps. It first accumulates elastic energy by using a latch-based system and then release the energy suddenly. In a recent innovative work, Bertoldi and coworkers [15] proposed a pneumatic

soft jumper by harnessing the snap-through instability of a semi-spherical shell. Recently, Wang *et al.* [31] reported an insect-scale jumping robot by leveraging a dynamic buckling cascade. For these existing soft jumpers, however, it remains a challenge to exactly control the direction and trajectory of jump. Directional locomotion can be realized through structural design with the asymmetrical deformation of soft robots. Zuo *et al.* [32] proposed a liquid crystal elastomer soft actuator capable of performing multi-directional crawling, based on the strategy that selective stimulation of specific domains of the actuator leads to various asymmetric deformation modes. By integrating multiple soft actuators as a whole, the system can be propelled to move in a specific direction [33]. This strategy has been employed to direct the locomotion of soft jumpers [18,28], which, however, requires an additional control system. However, these existing jumping actuation strategies pose some limitations in the control of jumping trajectory. For example, the combustion-based approach requires a precise volume ratio of the mixed gases for controlled explosions, while the latch-based approach limits to a rated output power.

Among the actuation methods [34,35], pneumatic soft actuators have emerged as a promising route to executing accurately controllable

* Corresponding author at: College of Mechanics and Engineering Science, Hohai University, Nanjing 210024, China.

** Corresponding author.

E-mail addresses: mli5@foxmail.com (M. Li), fengxq@tsinghua.edu.cn (X.-Q. Feng).

tasks [36]. Recently, Laake *et al.* [37] designed a novel semi-open pneumatic valve to realize sequential actuation of soft robots. In this paper, we propose a pneumatic soft actuator capable of directional jumping by harnessing the asymmetric snapping mechanism of a semi-spherical shell with a T-shaped crack. Systematic experiments and theoretical analysis are performed to demonstrate the efficacy and robustness of the designed soft robots. By presetting the initial inflation air pressure in the robot, its jumping trajectory can be precisely controlled. Finally, to highlight the maneuverability and high efficiency of the actuator, we showcase several applications, including jumping over obstacles of different heights and depths, escaping from a deep bottle, and moving across various challenging terrains.

2. Materials and methods

2.1. Design strategy of a directional soft jumper

The proposed pneumatic soft actuator comprises a short cylindrical tube, which is capped at the upper end by a flat plate with thickness t_u and has an inward semi-spherical shell at the lower end, as shown in Fig. 1A. It is fabricated by using the silicone rubber compression molding technology [38]. The detailed fabrication process is described in the [Supplementary Materials](#). Both the spherical shell and the cylindrical tube are made of silicone rubber (Dongjue Silicone NE 9370, China) with an initial shear modulus of $\mu = 2.0$ MPa. The top circular cover is made of silicone rubber (Dongjue Silicone NE 9340, China) with an initial shear modulus of $\mu = 0.5$ MPa. The shear moduli of the different parts can all be tuned in a wide range by changing the volume fractions of compositions in the silicone rubber.

Let t_o , h_o , and r_o denote the thickness, height, and inner radius of the outer cylindrical tube, respectively. The outer cylindrical tube connects to the inner spherical shell through a thin film with thickness t_f . The thickness, radius, and polar angle of the spherical shell are t_i , r_i , and θ , respectively. We cut a T-shaped, thickness-through incision in the spherical shell, with the two branches intersected at the center of the spherical shell. The two intersecting fissures of the T-incision have the lengths of l_1 and l_2 , respectively. The spherical shell is separated by the horizontal fissure of the T-shaped incision into two parts, F and B (Fig. 1A). Obviously, the whole system, including both F and B, is geometrically symmetric with respect to the vertical branch of the T-crack, but is asymmetric with respect to its horizontal branch. It is worth emphasizing that the incision of some other shapes could also be made, including a V-shaped one, which may also result in asymmetric deformations during snapping. We inflate the spacing encompassed by the cylindrical tube, the spherical shell and the circular cap with air.

2.2. Analysis of actuation mechanism

To reveal the energetic mechanism of the soft actuator, we first simulate its response to quasi-static inflation by using the commercial finite element software Abaqus. In our calculations, the model is discretized into C3D4H solid elements. The silicone rubber approximately obeys an incompressible neo-Hookean hyperelastic constitutive model. To simulate the inflating process, we apply the fluid cavity model and capture the pressure–volume curve by using the Riks method. More details of the finite element method (FEM) are available in the [Supplementary Materials](#). In the example, we take the following specific geometric parameters according to our experiments: $t_o = 1.0$ mm, $r_o = 10.6$ mm, $h_o = 9.3$ mm, $t_i = 1.5$ mm, $r_i = 10.0$ mm, $\theta = 60.0^\circ$, $t_f = 1.0$ mm, $t_u = 0.5$ mm, $l_1 = 4.0$ mm, and $l_2 = 4.0$ mm.

Our simulations show that the pressure–volume curve of the soft actuator shares a similar tendency to that of a spherical shell without the crack [15] (Fig. S4). Our soft actuator is also characterized by a limit of volume V_l (marked by the black square in Fig. 1B) when the internal air pressure increases to the value p_l . At this pressure, snapping-through instability occurs, causing the system to switch to a state with a lower

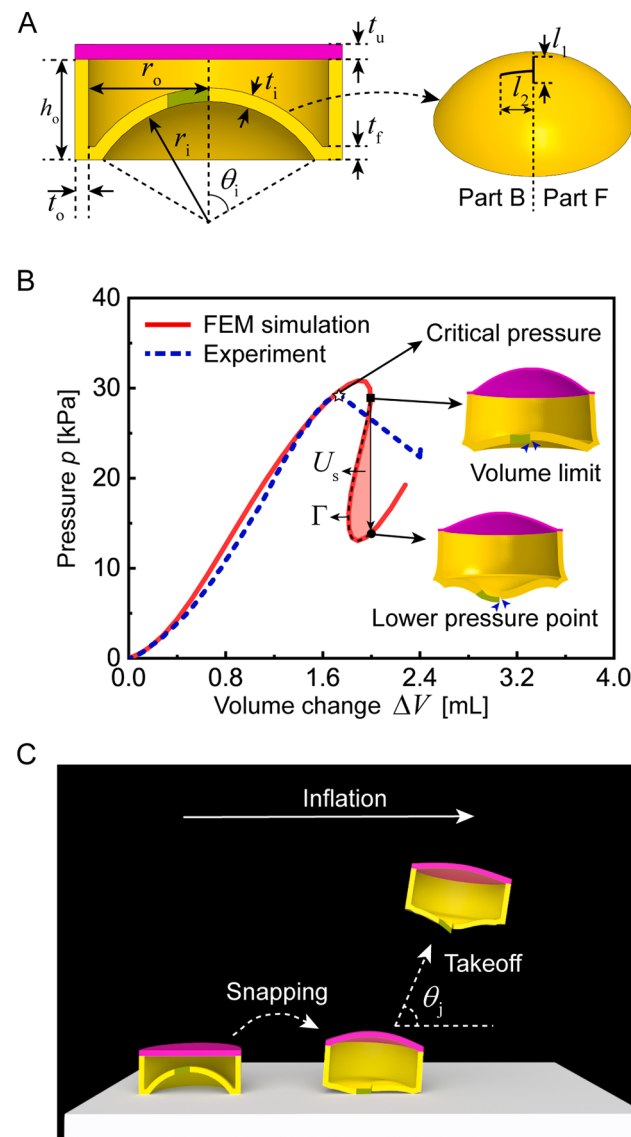


Fig. 1. Pneumatic soft jumper. (A) Geometry of the soft actuator, which comprises an inward semi-spherical shell with a T-shaped incision, a cylindrical tube, and an upper circular cap. It is divided into two parts, F and B. The shadow in the cross section of the shell denotes the incision. (B) The numerical (red) and experimental (blue) pressure–volume curves of the actuator subject to quasi-static air inflation. The curve obtained from FEM is characterized by a volume limit point (marked by the square), indicating the occurrence of snapping instability in the system. The snapping induces a sudden release of elastic energy U_s (marked by the jacinth area) [15,39,40]. In the experiment, the internal air pressure reaches a critical value p_c (marked by the star) and then drops quickly. During snapping, the soft actuator deforms asymmetrically due to the presence of the T-shaped crack in the shell. (C) Directional jumping locomotion of the actuator. The part B first impacts the ground, generating an inclined force to the actuator. Thus, the actuator takes off in the direction of θ_j measured from the ground.

pressure (marked by the black circle in Fig. 1B). During snapping, the originally-inward spherical shell inverts, characterized by the traveling path of the pole (marked by the blue arrows in Fig. 1B) of parts B and F. Different from the axisymmetric deformation of a spherical shell [15], the semi-spherical shell deforms asymmetrically due to the introduction of the crack. Parts B and F follow different paths during the geometric inversion, and B is lower than that F after snapping. The asymmetric impact between the actuator and the ground induces an inclined force, which creates a small torque with respect to the mass center of the

actuator, resulting in the tilting of the soft actuator. Therefore, the asymmetric impact supplies the soft actuator with an inclined force, which ultimately launches it along a certain direction (Fig. 1C).

The snapping of the actuator induces a sudden release of energy, U_s , corresponding to the pink highlighted area in Fig. 1B. It is calculated by

$$U_s = \int_{\Gamma} p d\Delta V, \quad (1)$$

where Γ is the equilibrium path from the point of the volume limit to that after snapping. For the soft actuator with the above parameters, we obtain $U_s = 0.54 \text{ J}$. The incision keeps closed before snapping and will open quickly due to the inversion of the spherical shell. With the opening of the incision, the inflated air swiftly ejects, propelling the shell to collide with the ground with a high velocity. The air ejection energy U_a also contributes to the kinetic energy of the actuator and thus enhances its jumping performance. Thus, the total energy U_t that drives the actuator comprises the released energy U_s and the air ejection energy U_a , that is,

$$U_t = U_s + U_a. \quad (2)$$

Importantly, after the release of high-pressure air, the shell will promptly regain its initial inward state. Therefore, the present pneumatic soft actuator is a semi-open pneumatic system that can switch on at the critical pressure and automatically return to its original state for the next jumping.

3. Results and discussions

3.1. Directional jump experiments

Now we experimentally investigate the jumping ability of the soft actuator fabricated in Fig. 1A. Air is inflated slowly into the actuator via a syringe pump (Longer, LSP01-2A), with a rate of 0.1 mL/s. The internal air pressure p is measured by using an air pressure gauge. Upon reaching 28 kPa, the soft actuator rapidly takes off, accompanied by a sudden drop of the internal pressure to 22 kPa (the blue dashed line in Fig. 1B). According to Eq. (3), the actuator's volume changes rapidly from 1.7 mL to 2.4 mL. At the beginning of jumping, part B inverts first and contacts with the ground, causing the actuator to rotate with an angle of about 5° (Fig. 2 and Movie S1). Subsequently, part B pushes against the ground (Fig. 2B–C), propelling the actuator to jump at an angle of 85° measured from the ground. The jump direction is determined by the initial tilt angle, which depends on both the configuration after snapping and the geometric parameters of the T-shaped incision. It is observed that it takes less than 6.5 ms from the beginning of snapping to the final launch.

Supplementary material related to this article can be found online at doi:10.1016/j.eml.2024.102242.

Supplementary material related to this article can be found online at doi:10.1016/j.eml.2024.102242.

The pressure–volume curve is plotted in Fig. 1B, where the abscissas ΔV denotes the volume change in the interior spacing of the actuator. Considering the compressibility of air, the volume change ΔV is approximately equal to the volume of the injected air minus the volume change due to the air compression. Thus, ΔV is calculated by [15]

$$\Delta V = \Delta V_{\text{syringe}} - \left(\frac{p - p_0}{p} \right) V_{\text{system}}, \quad (3)$$

where $\Delta V_{\text{syringe}}$ is the volume change injected by the syringe, V_{system} is the initial volume of the whole system (including the syringe and the actuator), and p_0 denotes the initial air pressure in the system. The experimental results show a good agreement with our simulations, with a small discrepancy that is attributed mainly to the manufacturing error and the lag in the pressure measurement.

To further illustrate the merits of the proposed semi-open pneumatic

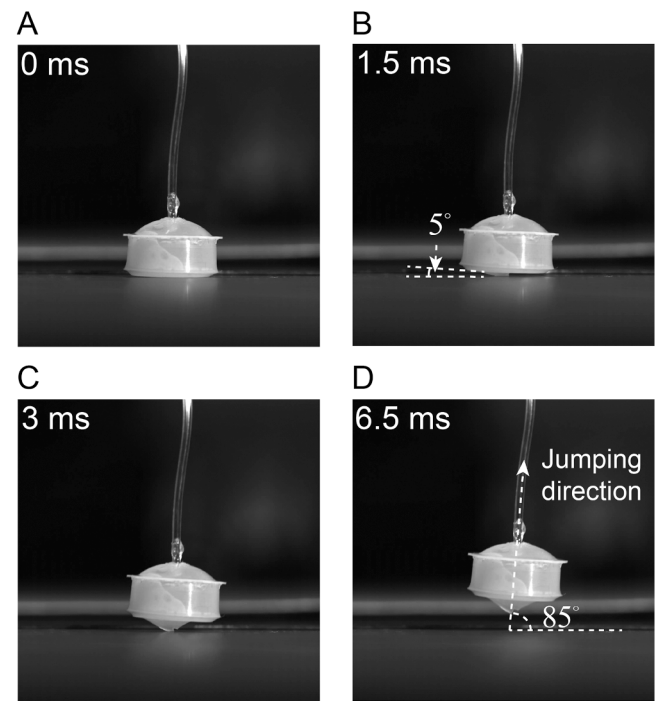


Fig. 2. Directional jumping locomotion of a soft jumper. (A)–(D) Experimental snapshots at 0.0, 1.5, 3.0, and 6.5 ms. (B) At the beginning of jumping, part B inverts and impacts the ground, tilting the actuator with an angle of 5°. (C) Then, part B pushes against the ground, propelling the actuator to jump. (D) Finally, the actuator launches at an angle of 85° measured from the ground.

system, we conduct both FEM simulations and experiments to compare the jumping behavior of two soft actuators, one having a T-shaped incision and the other having not. FEM simulations show that the pressure–volume curves of the two actuators are similar (Fig. S4). However, the experiments show that when slowly inflated at 0.1 mL/s, the soft actuator without the T-shaped incision cannot jump (Movie S2). This is because it is powered only by the elastic energy release induced by snapping, which is insufficient to drive the actuator to jump. Therefore, the semi-open pneumatic system can greatly improve the utilization of air energy. Additionally, it is highlighted that the air energy varies with the internal pressure and thereby we can realize the control of the total jumping energy U_t by changing the air pressure.

3.2. Accurate control of jumping trajectories

Inspired by the above findings, we use a pulse system (Fig. S5) to inflate the soft actuator rapidly with different initial air pressures $p_i = 30, 40, \text{ and } 50 \text{ kPa}$, which are all higher than the critical value of snapping, $p_c = 28 \text{ kPa}$. To track the jump trajectories, the location of the soft actuator is denoted by the centroid of the cylindrical shell. We observe that the jumping trajectories of the soft actuator vary dramatically under different preset air pressures (Fig. 3 and Movie S3), and thus we can tune the jumping direction and trajectory by changing the internal pressure. Because the air ejection energy depends on the preset air pressure, we assume that $U_a = cp_i V_i$, where c is a dissipation coefficient which can be determined by fitting the experimental results. Therefore, the total energy can be expressed as

$$U_t = U_s + U_a = \int_{\Gamma} pd\Delta V + cp_i V_i. \quad (4)$$

Specially, for the case of quasi-static inflation, the preset internal air pressure p_i is equal to the pressure limit p_1 at snapping, leading to $U_a = cp_1 V_i$.

Supplementary material related to this article can be found online at

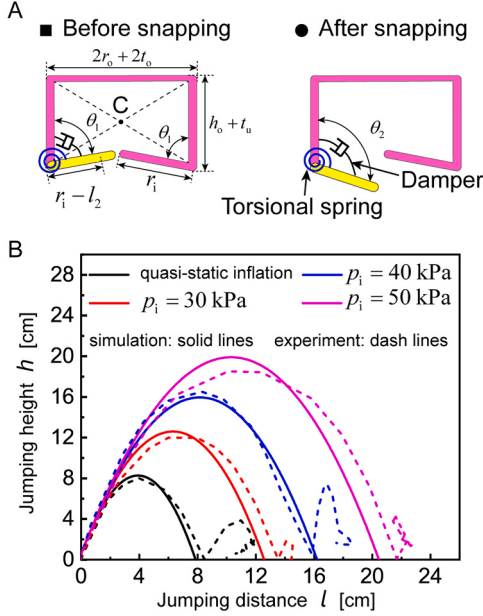


Fig. 3. Kinematic model of the soft actuator. (A) The kinematic model comprises a rigid frame and an active bar, connected with a torsional spring of stiffness k_{ts} . The torsional spring is pre-compressed before snapping and is stress-free after snapping, and thus the total energy U_t is stored in the torsional spring in the former configuration. We use the centroid C of the cylindrical tube to track the motion of the actuator. (B) Comparison of the trajectories of the point C during jumping between the experimental results and the theoretical predictions.

doi:10.1016/j.eml.2024.102242.

To further predict the jumping trajectory in terms of the design parameters, we develop a simplified two-dimensional kinematic model by using the commercial package Adams (More details of the method are available in the [Supplementary Materials](#)). The FEM simulation results are used as the input. As shown in Fig. 3A, the kinematic model comprises a rigid frame and an active bar, connected with a torsional spring with stiffness k_{ts} . The active bar with mass $m_i/2$ and length $r_i - l_2$ represents part B which impacts the ground during snapping. The rest of the soft jumper, including part F, the cylinder tube, and the circular cap, are modeled as a rigid frame since they will not impact the ground during the snapping. Assume that the torsional spring is pre-compressed before snapping and is stress-free after the impact, meaning that the total energy U_t is all stored in the torsional spring in the former configuration. Thus, the equivalent stiffness of the torsional spring is given by

$$k_{ts} = \frac{2U_t}{(\theta_2 - \theta_1)^2}, \quad (5)$$

where θ_1 and θ_2 are the angles between the bar and the rigid frame before and after snapping, respectively, which are determined from our FEM results. For the present actuator, FEM simulations give $\theta_1=78^\circ$ and $\theta_2=105^\circ$. To account for energy dissipation effects, the torsional spring is modeled with a damping coefficient c_t , which can be determined by fitting with the experimental results.

To validate the kinematic model, we compare the theoretically predicted jumping trajectory with the experimental measurements in four different situations, including under quasi-static inflation, and inflation under $p_i=30$, 40, and 50 kPa, respectively. The dynamic numerical results are shown in [Movie S3](#). A good agreement is found between the theoretical jumping trajectories and the experimental measurements, as shown in Fig. 3B, where we take the damping coefficient $c_t = 0.3 \text{ kg/s}$, and $c = 0.12$ for inflation under a preset air pressure and $c = 0.07$ for quasi-static inflation. It is noted that the parameter c is dependent on the geometric parameters of both the soft robot and the crack. The

discrepancy in the dissipation coefficient c between the two inflation modes can be attributed to the sudden release of air when inflated with high pressure. The results demonstrate that the kinematic model in Fig. 3 can well predict the jumping trajectory of the soft actuator. It is noted that the above kinematic method can predict the jumping trajectories of soft jumpers with different geometric parameters. Additionally, we find that in the case of quasi-static inflation, the ratio between the air ejection energy and the released elastic energy U_a/U_s reaches 426.3 %. The above experiments and model both confirm that the semi-open pneumatic system can greatly improve the utilization of air energy. Additionally, as the initial air pressure p_i increases, the soft jumper will jump higher and farther.

On the basis of the above results, we propose a precise strategy to control the jump trajectory of the soft actuator such that it can jump to the exact location or height. For a destination with given height and distance, for example, the above kinematic model can be used to calculate the air pressure required for the actuator to reach that position. This strategy will be demonstrated via a few different examples in the following section.

3.3. Jumping onto the top of a pillar

To verify the above-proposed control strategy, we inflate the soft actuator with different air pressures such that it can jump onto the tops of pillars with different distances l_b and heights h_b , as shown in [Fig. 4](#) and [Movie S4](#).

For a pillar with (l_b, h_b) , we first search for a jump trajectory of the soft actuator which contains the destination $(l_b + r_o, h_b + r_o)$ by using the kinematic model. The detailed search method is described in Section S5 of [Supplementary Materials](#). Then we can determine the required air pressure. Next, we inflate the soft jumper with the air pressure by presetting the pneumatic control system. Three examples of pillars are shown in [Fig. 4](#). For a pillar with smaller distance $l_b = 50 \text{ mm}$ and height $h_b = 50 \text{ mm}$, our calculation shows that only a slow rate of 0.1 mL/s is required. Our experiments show that the soft actuator can swiftly jump onto the pillar ([Fig. 4A](#)). For the two pillars with $(l_b = 70 \text{ mm}, h_b = 90 \text{ mm})$ and $(l_b = 80 \text{ mm}, h_b = 130 \text{ mm})$, the actuator can also easily jump onto the pillar tops when we set the air pressures $p_i = 31 \text{ kPa}$ and $p_i = 40 \text{ kPa}$, respectively ([Fig. 4B](#) and [C](#)).

When the ratio of the inner radius of the semi-spherical shell to its thickness is constant, both the released energy U_s and the gravitational potential energy are proportional to the mass [\[15\]](#). Therefore, by adjusting the inflation air pressure, the proposed soft jumper can be readily scaled to different sizes.

3.4. Adaptive jumping in various environments

In nature, some worms with soft-bodies, e.g., maggots [\[41\]](#), can jump swiftly to escape from dangerous environments or predators. Now we examine whether the soft actuator we have proposed can jump or not into and out of a deep bottle, which poses a challenge for most artificial soft robots. In our experiments, the bottle has a depth of 130 mm and a smaller opening of 52 mm diameter. It is found that the actuator can successfully achieve this task ([Movie S4](#), [Figs. 5A and 5B](#)). Therefore, the soft jumper can execute self-rescue from deep holes or other complex environments.

Furthermore, the proposed semi-open pneumatic system can achieve automatic resetting of the pneumatic system. After snapping, the actuator will return to the initial state automatically and quickly, leading to continuous jumping ([Movie S5](#)). The soft actuator exhibits the remarkable capability to not only effectively locomote across diverse complex terrains with sand, stones, trenches, and cobblestones ([Fig. 5C](#) and [Movie S6](#)), which may be uneven, low contact area, slippery, and even flowable, but also to jump out of the sand after being buried ([Fig. 5D](#) and [Movie S6](#)). There, the soft jump also has potential applications in planet exploration, in which the probe might be buried and move on complex

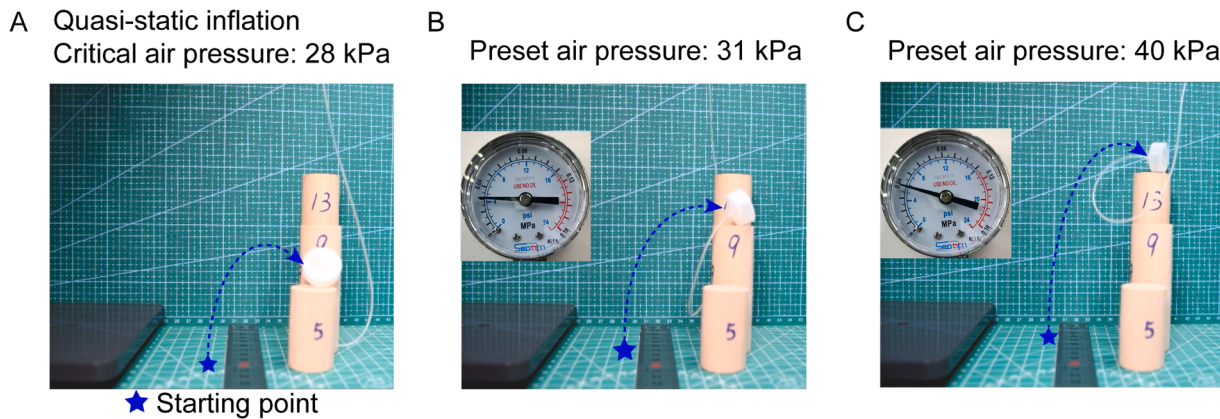


Fig. 4. An actuator jumps onto the tops of pillars of different distances and heights. (A) The actuator jumps onto a pillar with distance $l_b = 50$ mm and height $h_b = 50$ mm, where air is inflated with a slow, quasi-static rate of 0.1 mL/s. (B) The actuator jumps onto a pillar with $l_b = 70$ mm and $h_b = 90$ mm, where the air pressure is set to be $p_i = 31$ kPa. (C) For a pillar with $l_b = 80$ mm and $h_b = 130$ mm, we set the air pressure $p_i = 40$ kPa.

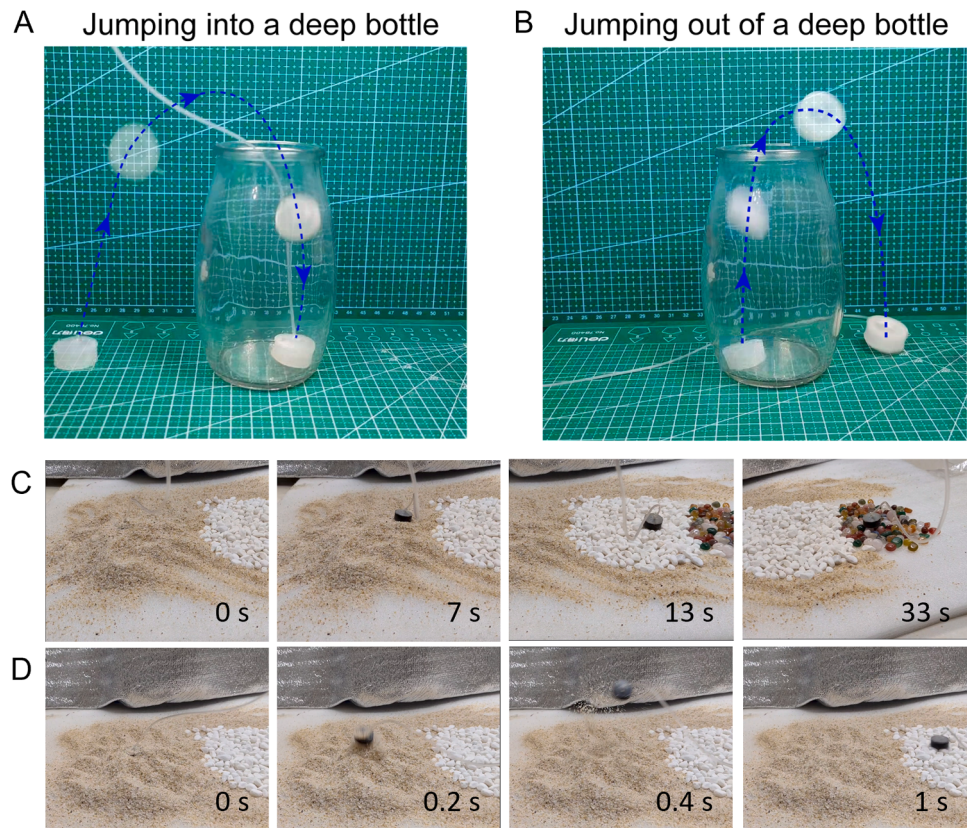


Fig. 5. An actuator jumps in various environments. (A) Jumping into and (B) out of a deep bottle, which has a height of 130 mm and a narrow opening of 52 mm diameter. (C) The soft actuator jumps across a variety of complex terrains: sand, stones (frictional and uneven), and cobblestones (slippery). (D) The buried soft actuator jumps out of the sand.

terrains.

4. Conclusions

In summary, we have proposed a pneumatic soft actuator that can jump in a controllable direction. The soft actuator comprises a semi-spherical shell with a T-shaped incision, which exhibits asymmetric snapping-through buckling when subjected to an increasing internal pressure. The asymmetric snapping results in an inclined impact with the ground, generating a force sufficiently large to drive the soft actuator to jump in a specific direction. Further, by supplying the actuator with a

preset air pressure, we realize precise control of the trajectory of the soft actuator. Functional jumping is demonstrated by several experiments, for examples, jumping onto platforms of varying heights, launching from uneven ground, and escaping from a bottle. The semi-open pneumatic system not only improves the utilization of air pressure, but also holds promise for automatic control of fluidic soft robots. This work offers a paradigmatic strategy for designing soft jumpers of various sizes which can efficiently traverse rough terrains.

Finally, it is also worth mentioning that since the soft jumper proposed in this paper is tethered, its jumping performance has some limitations. By integrating a micro air pump into the soft jumper or

supplying it with gas through chemical reaction, the soft jumper could be made untethered.

Data and materials availability

All data needed to evaluate the conclusions in the paper are present in the paper or the Supplementary Materials.

Funding

Research was supported by the National Natural Science Foundation of China (Grant Nos. 12002188, 11921002, and 12032014) and State Key Laboratory of Mechanics and Control for Aerospace Structures in Nanjing University of Aeronautics and Astronautics (No. MCMS-E-0123Y02).

CRediT authorship contribution statement

Wei Fang: Methodology, Formal analysis. **Xi-Qiao Feng:** Writing – review & editing, Supervision, Conceptualization. **Jian Wu:** Writing – review & editing. **Huikai Zhang:** Software, Methodology. **Min Li:** Writing – original draft, Methodology, Investigation, Formal analysis, Conceptualization.

Declaration of Competing Interest

The authors declare that they have no known competing financial interests or personal relationships that could have appeared to influence the work reported in this paper.

Data availability

Data will be made available on request.

Appendix A. Supporting information

Supplementary data associated with this article can be found in the online version at [doi:10.1016/j.eml.2024.102242](https://doi.org/10.1016/j.eml.2024.102242).

References

- [1] M. Runciman, A. Darzi, G.P. Mylonas, Soft robotics in minimally invasive surgery, *Soft Robot.* 6 (4) (2019) 423–443.
- [2] M. Cianchetti, C. Laschi, A. Menciassi, P. Dario, Biomedical applications of soft robotics, *Nat. Rev. Mater.* 3 (6) (2018) 143–153.
- [3] K.H.L. Heung, R.K.Y. Tong, A.T.H. Lau, Z. Li, Robotic glove with soft-elastic composite actuators for assisting activities of daily living, *Soft Robot.* 6 (2) (2019) 289–304.
- [4] B.B. Kang, H. Choi, H. Lee, K.J. Cho, Exo-Glove Poly II: a polymer-based soft wearable robot for the hand with a tendon-driven actuation system, *Soft Robot.* 6 (2) (2019) 214–227.
- [5] J. Shintake, V. Cacucciolo, D. Floreano, H. Shea, Soft robotic grippers, *Adv. Mater.* 30 (29) (2018) 33.
- [6] Z.X. Xie, A.G. Domel, N. An, C. Green, Z.Y. Gong, T.M. Wang, E.M. Knubben, J. C. Weaver, K. Bertoldi, L. Wen, Octopus arm-inspired tapered soft actuators with suckers for improved grasping, *Soft Robot.* 7 (5) (2020) 639–648.
- [7] G. Yin, Q. He, X. Zhou, Y. Wu, H. Li, M. Yu, Printing ionic polymer metal composite actuators by fused deposition modeling technology, *Int. J. Smart Nano Mater.* 12 (2) (2021) 218–231.
- [8] Y. Yang, Y. Wang, T. Yao, X. Feng, A flexible and smart shape memory alloy composite sheet based on efficient and bidirectional thermal management, *Int. J. Smart Nano Mater.* 13 (2) (2022) 315–329.
- [9] M.S. Verma, A. Ainala, D. Yang, D. Harburg, G.M. Whitesides, A soft tube-climbing robot, *Soft Robot.* 5 (2) (2018) 133–137.
- [10] R.F. Shepherd, F. Ilievski, W. Choi, S.A. Morin, A.A. Stokes, A.D. Mazzeo, X. Chen, M. Wang, G.M. Whitesides, Multigait soft robot, *Proc. Natl. Acad. Sci. USA* 108 (51) (2011) 20400–20403.
- [11] X.Y. Li, H.L. Duan, P.Y. Lv, X. Yi, Soft actuators based on liquid-vapor phase change composites, *Soft Robot.* 8 (3) (2020) 251–261.
- [12] Y. Guo, J. Guo, L. Liu, Y. Liu, J. Leng, Bioinspired multimodal soft robot driven by a single dielectric elastomer actuator and two flexible electroadhesive feet, *Extrem. Mech. Lett.* 53 (2022) 101720.
- [13] M. Duduta, F.C.J. Berlinger, R. Nagpal, D.R. Clarke, R.J. Wood, F.Z. Temel, Electrically-latched compliant jumping mechanism based on a dielectric elastomer actuator, *Smart Mater. Struct.* 28 (9) (2019) 8.
- [14] W.Q. Hu, G.Z. Lum, M. Mastrangeli, M. Sitti, Small-scale soft-bodied robot with multimodal locomotion, *Nature* 554 (7690) (2018) 81–85.
- [15] B. Gorissen, D. Melancon, N. Vasios, M. Torbati, K. Bertoldi, Inflatable soft jumper inspired by shell snapping, *Sci. Robot.* 5 (42) (2020) 7.
- [16] C.Y. Ahn, X.D. Liang, S.Q. Cai, Bioinspired design of light-powered crawling, squeezing, and jumping untethered soft robot, *Adv. Mater. Technol.* 4 (7) (2019) 9.
- [17] S.G. Li, D. Rus, JelloCube: a continuously jumping robot with soft body, *Ieee-Asme Trans. Mechatron.* 24 (2) (2019) 447–458.
- [18] R. Chen, Z. Yuan, J. Guo, L. Bai, X. Zhu, F. Liu, H. Pu, L. Xin, Y. Peng, J. Luo, L. Wen, Y. Sun, Legless soft robots capable of rapid, continuous, and steered jumping, *Nat. Commun.* 12 (1) (2021) 7028.
- [19] Y.C. Tang, Y.D. Chi, J.F. Sun, Z.H. Huang, O.H. Maghsoudi, A. Spence, J.G. Zhao, H. Su, J. Yin, Leveraging elastic instabilities for amplified performance: Spine-inspired high-speed and high-force soft robots, *Sci. Adv.* 6 (19) (2020) 12.
- [20] J.W. Zhao, J.M. Zhang, D. McCou, Z.G. Hao, S. Wang, X.B. Wang, B. Huang, L. N. Sun, Soft and fast hopping-running robot with speed of six times its body length per second, *Soft Robot.* 6 (6) (2019) 713–721.
- [21] H.T. Lin, G.G. Leisk, B. Trimmer, GoQBot: a caterpillar-inspired soft-bodied rolling robot, *Bioinspiration Biomim.* 6 (2) (2011) 14.
- [22] Z.J. Wang, K. Li, Q.G. He, S.Q. Cai, A light-powered ultralight tensegrity robot with high deformability and load capacity, *Adv. Mater.* 31 (7) (2019) 8.
- [23] T.F. Li, G.R. Li, Y.M. Liang, T.Y. Cheng, J. Dai, X.X. Yang, B.Y. Liu, Z.D. Zeng, Z. L. Huang, Y.W. Luo, T. Xie, W. Yang, Fast-moving soft electronic fish, *Sci. Adv.* 3 (4) (2017) 7.
- [24] Z.Y. Ren, W.Q. Hu, X.G. Dong, M. Sitti, Multi-functional soft-bodied jellyfish-like swimming, *Nat. Commun.* 10 (2019) 12.
- [25] Z.M. Hu, W. Fang, Q.Y. Li, X.Q. Feng, J.A. Lv, Optocapillarity-driven assembly and reconfiguration of liquid crystal polymer actuators, *Nat. Commun.* 11 (1) (2020) 5780.
- [26] S. Yin, Z. Jia, X. Li, J. Zhu, Y. Xu, T. Li, Machine-learning-accelerated design of functional structural components in deep-sea soft robots, *Extrem. Mech. Lett.* 52 (2022) 101635.
- [27] R.F. Shepherd, A.A. Stokes, J. Freake, J. Barber, P.W. Snyder, A.D. Mazzeo, L. Cademartiri, S.A. Morin, G.M. Whitesides, Using explosions to power a soft robot, *Angew. Chem. -Int. Ed.* 52 (10) (2013) 2892–2896.
- [28] N.W. Bartlett, M.T. Tolley, J.T.B. Overvelde, J.C. Weaver, B. Mosadegh, K. Bertoldi, G.M. Whitesides, R.J. Wood, A 3D-printed, functionally graded soft robot powered by combustion, *Science* 349 (6244) (2015) 161–165.
- [29] M. Loepfe, C.M. Schumacher, U.B. Lustenberger, W.J. Stark, An untethered, jumping poly-poly soft robot driven by combustion, *Soft Robot.* 2 (1) (2015) 33–41.
- [30] A.M. Abdulla, P.V. Braun, K.J. Hsia, Programmable shape transformation of elastic spherical domes, *Soft Matter* 12 (29) (2016) 6184–6195.
- [31] Y. Wang, Q. Wang, M. Liu, Y. Qin, L. Cheng, O. Bolmin, M. Alleyne, A. Wissa, R. Baughman, D. Vella, S. Tawfick, Insect-scale jumping robots enabled by a dynamic buckling cascade, *Proc. Natl. Acad. Sci. USA* 120 (2023) e2210651120.
- [32] B. Zuo, M. Wang, B.-P. Lin, H. Yang, Visible and infrared three-wavelength modulated multi-directional actuators, *Nat. Commun.* 10 (1) (2019) 4539.
- [33] L. Qin, X.Q. Liang, H. Huang, C.K. Chui, R.C.H. Yeow, J. Zhu, A versatile soft crawling robot with rapid locomotion, *Soft Robot.* 6 (4) (2019) 455–467.
- [34] L. Yao, H. Yan, Y. He, N. Zhao, X. Wang, C. Li, L. Sun, Y. He, Y. Liu, J. Zhang, Actuation performances of catkin fibers reinforced thiol-acrylate main-chain liquid crystalline elastomer, *Int. J. Smart Nano Mater.* 13 (4) (2022) 668–690.
- [35] Z. Zhu, C. Bian, W. Bai, Q. Hu, S. Chen, Integrated fabrication process with multiple optimized factors for high power density of IPMC actuator, *Int. J. Smart Nano Mater.* 13 (4) (2022) 643–667.
- [36] D. Rus, M.T. Tolley, Design, fabrication and control of soft robots, *Nature* 521 (7553) (2015) 467–475.
- [37] L.C. van Laake, J. de Vries, S.M. Kani, J.T.B. Overvelde, A fluidic relaxation oscillator for reprogrammable sequential actuation in soft robots, *Mater.* 5 (9) (2022) 2898–2917.
- [38] A.X. Kohll, N.H. Cohrs, R. Walker, A. Petrou, M. Loepfe, M.S. Daners, V. Falk, M. Meboldt, W.J. Stark, Long-term performance of a pneumatically actuated soft pump manufactured by rubber compression molding, *Soft Robot.* 6 (2) (2019) 206–213.
- [39] A. Lee, F. López Jiménez, J. Marthelot, J.W. Hutchinson, P.M. Reis, The geometric role of precisely engineered imperfections on the critical buckling load of spherical elastic shells, *J. Appl. Mech.* 83 (11) (2016) 111005.
- [40] J.W. Hutchinson, Buckling of spherical shells revisited, *Proc. R. Soc. A* 472 (2195) (2016) 20160577.
- [41] G.M. Farley, M.J. Wise, J.S. Harrison, G.P. Sutton, C. Kuo, S.N. Patek, Adhesive latching and legless leaping in small, worm-like insect larvae, *J. Exp. Biol.* 222 (15) (2019) 12.